Analysis and Optimization of a Phase Shifter Controlled by a Piezoelectric Transducer

Tae-Yeoul Yun, *Student Member, IEEE*, and Kai Chang, *Fellow, IEEE*

***Abstract*—This paper introduces a method for analyzing and optimizing a phase shifter controlled by a piezoelectric transducer (PET). To analyze the multilayer microstrip structure of the PET-controlled phase shifter, new equivalent single-layer (ESL) equations for the phase shift and loss calculations are developed and confirmed with spectral-domain analysis (SDA) of the moment method. A parametric analysis is accomplished with ESL equations and SDA, and optimization guidelines are suggested. An optimized PET phase shifter is demonstrated to operate up to 40 GHz with a maximum total loss of 4 dB and phase shift of 480°. Measured results agree very well with calculations showing substantially smaller control voltage, size, and dispersion, as compared to previously published data. This new analysis and optimization technique for the PET-controlled phase shifter should be useful in the design of phased-array antennas and tunable microwave circuits.**

***Index Terms*—Multilayer microstrip, perturbation, phase shifter, piezoelectric transducer.**

I. Introduction

A WIDE-BAND and low-loss phase shifter is often required for beam steering and beam forming in phased-array antenna systems, as well as timing recovery circuits and phase equalizers for data channels. Since phased-array antennas typically consist of several thousands of phase shifters, the amount of which is about 45% of the total system expense, low cost and low-complexity phase-shifter designs are very important issues [1]. Published results on monolithic microwave integrated circuit (MMIC) [2], ferroelectric [3], solid-state [4], and photonically controlled [5] phase shifters are typically narrow-band, lossy, or providing only a small phase shift. Recently, a new phase shifter was presented using dielectric image-line perturbation at Ka-band [6]. This idea can be improved by replacing the image-line with a microstrip line. The use of microstrip line is very useful because of its quasi-TEM mode without cutoff frequency and easy fabrication with no waveguide transition required. Other transmission lines such as a coplanar waveguide, coplanar strip, and slot line can also be employed. A dielectric or metal plate perturbs the electromagnetic fields of the transmission line. This perturbation changes the distributed capacitance, which corresponds to a variation of the effective permittivity and propagation constant and, thus, the phase shift. The characteristic impedance (Z_c) is only slightly affected and no additionally impedance-matching circuit is required for broad-band operation [7].

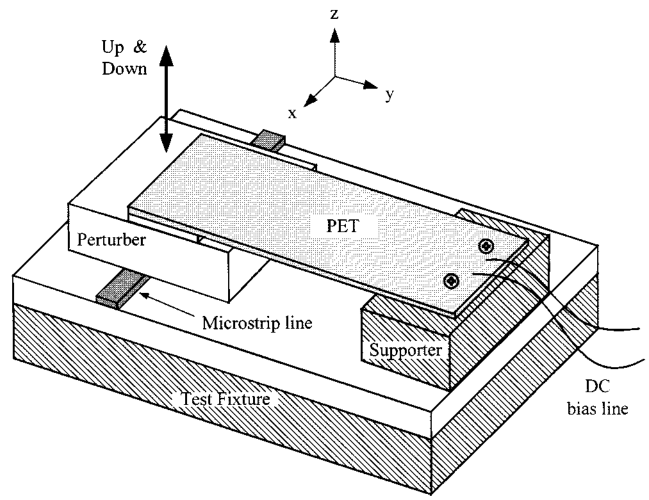

(a)

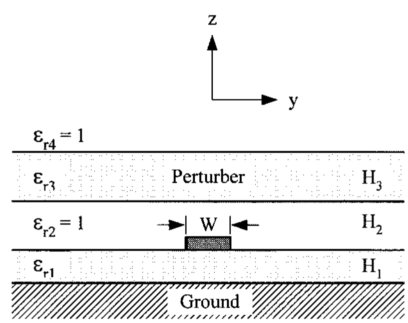

(b)

Fig. 1. New phase shifter controlled by a PET on a microstrip line. (a) Configuration. (b) Microstrip-line-like multilayer structure.

Three perturbation methods for phase shifting are possible. The perturber may move horizontally in the y-axis direction and rotate or move vertically in the z-axis direction, as shown in Fig. 1. The feasibility of phase shifting with the vertical movement was successfully demonstrated using a metal-disc perturber regulated manually by a micrometer head [6]. In this paper, rather than using manual control, a piezoelectric transducer (PET) or piezoelectric actuator is used to control the perturber vertically along the z-axis, as shown in Fig. 1(a). The PET is a piezoelectric ceramic, deflected by an applied voltage [8]. A thin-metal shim is centered and connected to one polarity of the dc control voltage. The center shim is sandwiched by two opposite poled piezoelectric ceramics, which are connected with the

Manuscript received November 30, 2000. This work was supported in part by the National Science Foundation and by the U.S. Air Force.

The authors are with the Department of Electrical Engineering, Texas A&M University, College Station, TX 77843-3128 USA (e-mail: chang@ee.tamu.edu).

Publisher Item Identifier S 0018-9480(02)00021-2.

other polarity. The perturber attached to the PET may consist of metal, dielectric, or metal-covered dielectric. Since the dielectric perturber experimentally showed the lowest loss, only the dielectric perturber is used in this paper.

The new PET-controlled phase shifter, its applications for the voltage tuned resonator, and the low-cost multiline phase shifter for the phased-array antenna were recently reported [7], [9], [10]. The calculated results in these papers were based on static variational analysis without considering the dispersive characteristic of a multilayer microstrip line. The variational analysis results did not agree very well with measurement at frequencies above about 10 GHz [10]. This paper proposes new dispersion formulas and a parametric analysis for the multilayer microstrip structure of the PET phase shifter. These new equations are confirmed with experimental results and the spectral-domain analysis (SDA) of the moment method [11]. From the parametric analysis, an optimum PET phase shifter is designed and measured, which shows much improved results compared with the previously reported data [7], [9], [10] and comparable results with distributed varactor and microelectromechanical system (MEMS) phase shifters [12]–[15]. The PET-controlled phase shifter and its simple method of analysis should be useful in microwave and millimeter-wave applications.

II. Formulation of Frequency-Dependent Phase Shift

The microstrip transmission line is dispersive in nature. Many rigorous theoretical formulations have been reported in the literature to characterize the dispersion effect of the multilayer structure of the microstrip line [16]–[18]. However, such formulations require accurate full-wave field analyses that are not directly suitable for use in computer-aided design (CAD). Closed-form dispersion models for specific multilayer microstrip structures have been proposed [19] using the Kirschning–Jansen (K–J) model [20] with an equivalent single-layer substrate. This analysis adequately characterized the dispersion effect of the shielded microstrip line, suspended microstrip line, composite substrate, and shielded composite-substrate microstrip line. However, the structure of the PET phase shifter, shown in Fig. 1(b), consisting of a substrate (relative permittivity ε_{r1}), microstrip line, air gap ($\varepsilon_{r2} = 1$), and perturber (ε_{r3}), requires new closed-form models because it is different from those configurations previously analyzed. Dielectric and metal losses and PET deflection equations are also included in the analysis.

A. Equivalent-Single-Layer Dispersion Model

The differential phase shift $\Delta\phi$ caused by the perturbation is calculated as

$$\Delta\phi = L_p \cdot \Delta\beta \tag{1}$$

where L_p is the length of perturber and $\Delta\beta$, the difference between the unperturbed and perturbed propagation constants along the microstrip line, is given by

$$\Delta\beta = \frac{2\pi}{\lambda_o}\left(\sqrt{\varepsilon'_{\text{eff}}(f)} - \sqrt{\varepsilon_{\text{eff}}(f)}\right) \tag{2}$$

where λ_0 is the wavelength in free space, f is the frequency, and $\varepsilon_{\text{eff}}(f)$ and $\varepsilon'_{\text{eff}}(f)$ are the effective relative permittivities of the perturbed ($\varepsilon_{r3} \neq 1$) and unperturbed ($\varepsilon_{r3} = 1$) microstrip, respectively. $\varepsilon'_{\text{eff}}(f)$ is calculated from the K–J closed-form formula. However, there are no closed-form equations for $\varepsilon_{\text{eff}}(f)$ and, therefore, it is calculated by the following theoretical and empirical derivation procedure. The modified K–J formula for the multilayer microstrip-line dispersion equation is given by

$$\varepsilon_{\text{eff}}(f) = \varepsilon_{\text{eq}}(f) - \frac{\varepsilon_{\text{eq}}(f) - \varepsilon_{\text{eff}}(0)}{1 + P(f)} \tag{3}$$

where $\varepsilon_{\text{eq}}(f)$ is the frequency-dependent equivalent single-layer (ESL) relative permittivity, $P(f)$ is the frequency-dependent term of the K–J formula, which is dependent on W/H_1, $f \cdot H_1$, and $\varepsilon_{\text{eq}}(f)$ [20]. The static quasi-TEM effective permittivity $\varepsilon_{\text{eff}}(0)$ and characteristic impedance $Z_c(0)$ are obtained by calculation of the static line capacitances using variational analysis with the transverse transmission-line (TTL) method [21]–[23].

Using these results for $\varepsilon_{\text{eff}}(0)$, $\varepsilon_{\text{eq}}(0)$, and $Z_c(0)$, the ESL permittivity $\varepsilon_{\text{eq}}(f)$ is obtained by iterative optimization, which is finally given by

$$\varepsilon_{\text{eq}}(f) = \varepsilon_{\text{eq}}(0) - \frac{\varepsilon_{\text{eq}}(0) - \varepsilon_{rl}}{0.95 + \left(\frac{f_p}{1.2f}\right)^{(\varepsilon_{rl}/\varepsilon_{rs})\cdot\sqrt[4]{(H_3/2H_1)}}} \tag{4}$$

$$f_p = \frac{Z_c(0)}{2\mu_o H_1\sqrt{\varepsilon_{\text{eff}}(0)}} - \frac{H_2}{H_1} f^{1.2} \tag{5}$$

where ε_{rl} is the larger relative permittivity, ε_{rs} is the smaller one between ε_{r1} and ε_{r3}, and μ_0 is the permeability in free space in units of henry/millimeter. f_p is set to zero if it is less than zero.

Equations (4) and (5) of $\varepsilon_{\text{eq}}(f)$ are found from the following. As the frequency decreases, $\varepsilon_{\text{eq}}(f)$ approaches $\varepsilon_{\text{eq}}(0)$, which can be calculated from [24]. As the frequency increases, $\varepsilon_{\text{eq}}(f)$ approaches the larger permittivity (ε_{rl}) between ε_{r1} and ε_{r3}. Using an inflation frequency f_p [25] as a frequency normalization factor, the basic form is $\varepsilon_{\text{eq}}(f) = \varepsilon_{\text{eq}}(0) - (\varepsilon_{\text{eq}}(0) - \varepsilon_{rl})/(1 + f_p/f)$. The original f_p had only the first term in (5), which includes the effects of the linewidth (indirectly from $Z_c(0)$), substrate thickness (H_1), and substrate permittivity (indirectly from $\varepsilon_{\text{eff}}(0)$). A second term is added to account for the decrease in the inflation frequency as the air gap H_2 increases. The perturber permittivity and thickness variation effects are considered as ratio forms. Several constant numbers were obtained from trial and error.

The new ESL equations for the PET-controlled phase shifter, i.e., (3)–(5), are optimized to operate over $2.33 \leq (\varepsilon_{r1}\ or\ \varepsilon_{r3}) \leq 10.8$, $0.5 \leq W/H_1 \leq 1.55$, $H_3/H_1 \geq 0.6$, and $f \leq 40$ GHz, for the dielectric perturber. Each range of parameters will be used for the following parametric analysis. The accuracy of the ESL dispersion model was verified by comparing with SDA [11] data as follows:

$$\text{accuracy} = \sqrt{\frac{1}{N}\sum_{n=1}^{N}\left\{\frac{(\varepsilon_{\text{effSDA}_n} - \varepsilon_{\text{effESL}_n})}{\varepsilon_{\text{effSDA}_n}}\right\}^2}. \tag{6}$$

Obtained rms accuracy over 160 points is 1.65%.

B. Losses

Most losses are contributed by dielectric and conductor losses assuming that the radiation loss is small because of the perturber

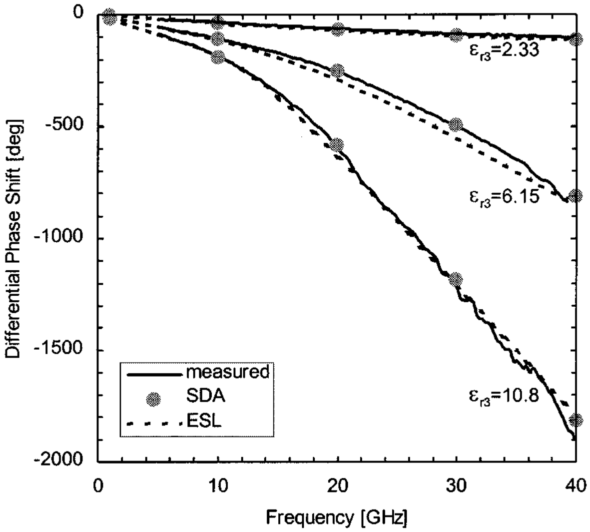

(a)

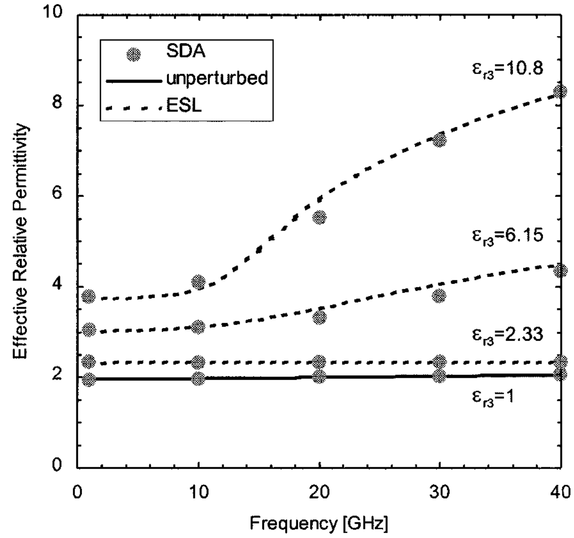

(b)

Fig. 2. Dielectric perturbation with no air gap ($H_2 = 0$), $\varepsilon_{r3} = 2.33/6.15/10.8$, $H_3 = 125/50/50$ mil, $L_p = 1.03$ in, $\varepsilon_{r1} = 2.33$, $H_1 = 20$ mil, and $W = 22$ mil. (a) Differential phase shift. (b) Effective relative permittivity.

overlay. The dielectric loss caused by the finite conductivity of the dielectric layers is given by

$$\alpha_d = \frac{27.3}{\lambda_o\sqrt{\varepsilon_{\text{eff}}}}\left\{\left(\frac{\varepsilon'_{\text{eff}}-1}{\varepsilon_{r1}-1}\right)\varepsilon_{r1}\tan\delta_1 + \left(\frac{\varepsilon_{\text{eff}}-\varepsilon'_{\text{eff}}}{\varepsilon_{r3}-1}\right)\varepsilon_{r3}\tan\delta_3\right\} \quad (7)$$

where static values are used for all relative permittivities (ε_{eff}, $\varepsilon'_{\text{eff}}$, ε_{r1}, and ε_{r3}) [26], and $\tan\delta_1$ and $\tan\delta_3$ are the loss tangents of the substrate and perturber, respectively.

The conductor loss α_c is obtained from [27]

$$\alpha_c = \frac{1}{2\mu_o Z_c}\sum_j R_{sj}\frac{\partial L}{\partial n_j} \quad (8)$$

where L denotes the inductance of the microstrip, $\partial L/\partial n_j$ is the derivative of L with respect to the incremental recession of the conductor wall j, n_j is the vector normal to this wall, and R_{sj} is the surface resistance of the wall j. α_c is modified by a correction factor due to the strip roughness [28] as

$$\alpha'_c = \alpha_c\left[1+\frac{2}{\pi}\tan^{-1}\left\{1.4\left(\frac{\Delta}{\delta_s}\right)^2\right\}\right] \quad (9)$$

where δ_s is the skin depth and Δ is the rms surface roughness. The final form of the loss calculation is a function of W, H_1, metal thickness, strip conductivity, frequency, Z_c of the multilayer microstrip line, and strip metal surface roughness. The total loss in unit of decibels for a perturbed length of L_P is given by

$$\text{Loss} = (\alpha'_c + \alpha_d)L_p. \quad (10)$$

C. Characteristic Impedance and Deflection of PET

An approximate calculation for the frequency-dependent characteristic impedance is used from [28]

$$Z_c(f) = Z_c(0)\frac{\varepsilon_{\text{eff}}(f)-1}{\varepsilon_{\text{eff}}(0)-1}\sqrt{\frac{\varepsilon_{\text{eff}}(0)}{\varepsilon_{\text{eff}}(f)}}. \quad (11)$$

The PET plate or cantilever is composed of two oppositely poled plates. The deflection h at the end of the cantilever is given by [8]

$$h = 4d_{31}\frac{L^2}{t^2}V \quad (12)$$

where d_{31} is the mechanical strain coefficient of 2.81×10^{-7} mm/V, V is the applied voltage, L is the length of PET, and t is the thickness of PET, are 57.2 and 0.5 mm, respectively. The deflection (h) or air gap (H_2) linearly depends on the PET control voltage.

III. Properties of PET Phase Shifter

The substrates used for the following experiments and calculations are RT/Duroid 5870 and 6010.8 with ε_{r1} of 2.33 and 10.8, H_1 of 20 and 25 mil, and W of 50 and 22 mil, respectively. The microstrip linewidths are designed for a characteristic impedance (Z_c) of more than 55 Ω to compensate for the decrease due to dielectric perturbation. At the maximum perturbation, i.e., when the dielectric perturber is placed on the microstrip line, Z_c is close to 50 Ω. With its supporter, the PET has a size of 2.75 in × 1.25 in × 0.085 in with a composition of lead–zirconate–titanate (PZT) and can be deflected over ±1.325 mm at ±90 V.

A. Parametric Analysis

In Fig. 2, the effects of three different dielectric perturbers are analyzed. For $\varepsilon_{r3} > \varepsilon_{r1}$ with $H_2 = 0$, the previous model [29] did not account for the inversion of power that flows from substrate to superstrate. As shown in Fig. 2(a), the proposed ESL model shows very good accuracy in comparison with measured and SDA results for the differential phase shift. These results predict that a higher perturber permittivity results in a larger phase shift without air gap ($H_2 = 0$). The effective dielectric constants in Fig. 2(b) agree very well with SDA results. The effective dielectric constant moves close to ε_{r3} as the frequency increases. The small difference between measurements and calculations may be due, in part, to the fact that the nonzero metal

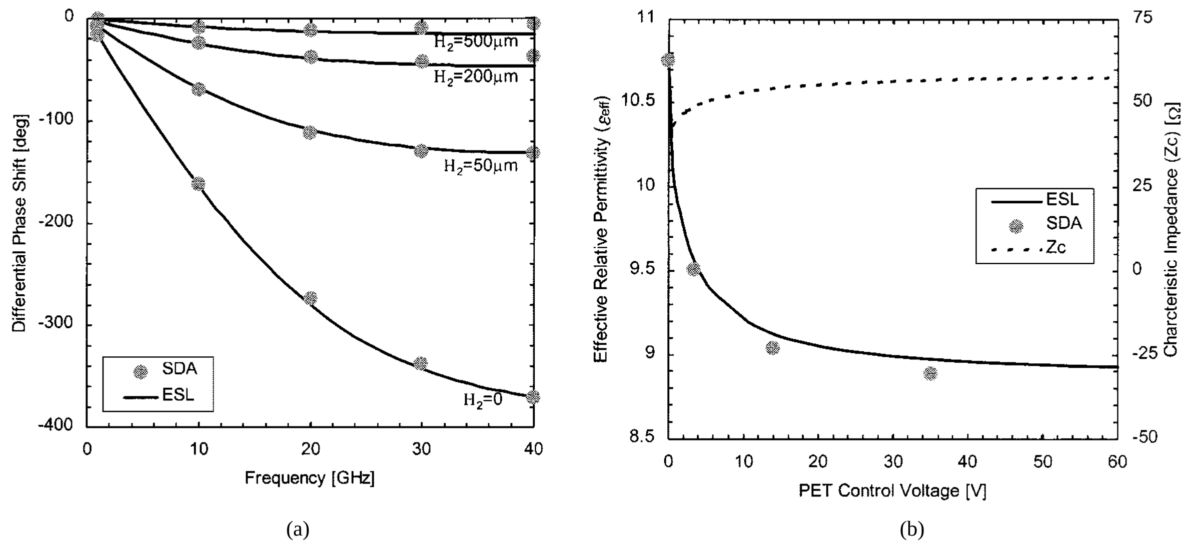

Fig. 3. Effect of the air gap (H_2) with $\varepsilon_{r3} = 10.8$, $H_2 = 0/50/200/500\ \mu$m (corresponds to PET voltage of 0/3.4/13.6/34 V), $H_3 = 50$ mil, $L_p = 1.0$ in, $\varepsilon_{r1} = 10.8$, $H_1 = 25$ mil, and $W = 22$ mil. (a) Phase shift versus frequency. (b) Effective relative permittivity and characteristic impedance versus PET voltage at 40 GHz.

thickness, the frequency-dependent variation of the dielectric constant for the real substrate and perturber, and the discontinuity at the boundary of the perturber are not considered in calculations.

The variation of the air gap is investigated in Fig. 3. Curved data lines are caused by the dispersion. The characteristic impedance Z_c is found to be relatively insensitive to the air-gap variation, which gives fairly good impedance matching without the requirement of matching networks. This is a major advantage of this type of phase shifter. Even so, the effective dielectric constant drastically changes with the air-gap variation, which results in a significant phase change. In this case, the most phase shift occurs with H_2 less than 500 μm, which corresponds to the PET control voltage of less than 35 V. Varying perturber thickness also slightly affects the phase shift, as shown in Fig. 4. The thin dielectric perturber allows part of the electric field to be in the air above the perturber. Thus, the effective dielectric constant and phase shifting are not as significantly increased as with the thicker perturber. The thicker perturber produces the larger phase shifts. However, the phase shift is not improved much beyond $H_3/H_1 \geq 2$ because, in that case, most of the electric fields are confined within the substrate and perturber. In addition, the thicker perturber requires a higher PET control voltage for the phase shift closer to zero. The strip width W strongly affects the phase shift at 0 V, as shown in Fig. 5(a) for the fixed values of H_1. The narrower strip width results in a larger phase shift, caused by the smaller effective permittivity $\varepsilon'_{\text{eff}}(f)$. Unfortunately, the larger phase shift is paid for with a larger Z_c, thus degrading the return loss. For one of the most important parametric analyses, Fig. 5(b) shows the effect of varying the substrate thickness H_1 with the width W designed to maintain a characteristic impedance of about 55 Ω. As H_1 decreases while $Z_c(0)$ is maintained at 55 Ω, the phase shift is much improved without degrading . One more advantage obtained is, for example, the possibility of decreasing the control voltage to around 10 V. This voltage can be improved with more optimizations in other parameters.

From the above parametric analysis, the phase shift can be maximized by having: 1) higher permittivity of substrate and perturber (ε_{r1} and ε_{r3}); 2) thicker perturber ($H_3/H_1 \geq 2$); 3) narrower strip width (W); and 4) thinner substrate (H_1).

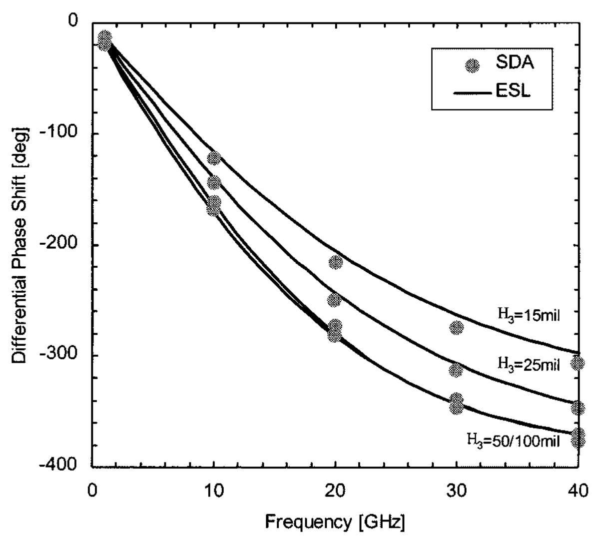

Fig. 4. Variation of dielectric perturber thickness with $\varepsilon_{r3} = 10.8$, $H_3 = 15/25/50/100$ mil, $L_p = 1.0$ in, $\varepsilon_{r1} = 10.8$, $H_1 = 25$ mil, $H_2 = 0$, and $W = 22$ mil.

In addition, having a higher permittivity of the perturber ε_{r3} than that of the substrate ε_{r1} should tremendously increase the amount of phase shift. However, in this case, it is possible to degrade the phase-shifter performance by becoming very lossy at a high-frequency range due to leaky-wave-mode generation [17]

B. Hysteresis Loop

The hysteresis loop is a very important electrical characteristic of the ferroelectric ceramic material used to fabricate the PET. The PET deflection of (12) and PET control voltage responses in the preceding analysis were assumed without hysteresis. The real PET phase shifter shows a hysteresis characteristic. There are two curves depending on the control voltage

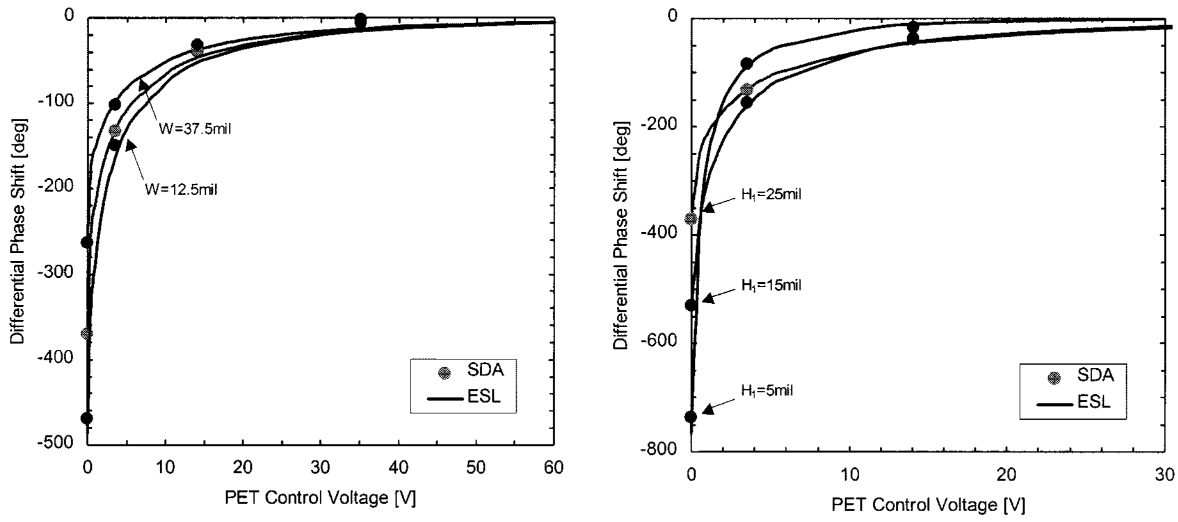

(a) (b)

Fig. 5. Phase shifts at 40 GHz with $\varepsilon_{r3} = 10.8$, $H_3 = 50$ mil, $L_p = 1.0$ in, and $\varepsilon_{r3} = 10.8$. (a) Strip-width effect with $H_1 = 25$ mil, $W = 12.5/22/37.5$ mil, and $W/H_1 = 0.5/0.88/1.55$. (b) Substrate thickness effect with $H_1 = 5/15/25$ mil, $W = 3.3/12.4/22$ mil, and $W/H_1 = 0.66/0.83/0.88$.

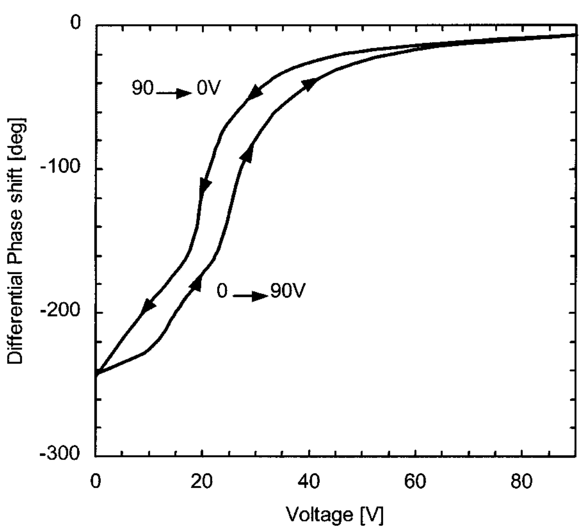

Fig. 6. Measured hysteresis loop of the PET phase shifter at 10 GHz.

direction, i.e., up or down, as shown in Fig. 6. This phenomenon may be measured by the Sawyer–Tower method or others at a very low frequency of less than 100 Hz [8]. The proposed phase shifter controlled by PET can be used as a new method for measuring the hysteresis at high frequency. However, the hysteresis may not be desirable for some applications. There are several ways to escape it. First, in the lanthanum-modified PZT material ($Pb_{1-x}La_x(Zr_yTi_{1-y})_{1-x/4}O_3$, PLZT) system, different composition ratios exhibit diverse shapes of the hysteresis loop. This means that the hysteresis loop can be illustrated as one curve or straight line for a specific composition. The smaller deflection is, however, a tradeoff to pay for it. This method depends on the material itself without external circuit. Another method was suggested using external proportional, integral, and differential (PID) control or compensation circuits [30], [31]. This paper does not deal with these antihysteresis methods, as well as aging and temperature effects. In the two paths of the hysteresis loop, the transition curve going from 0 to 90 V was used in our experiments.

IV. Optimized Results

The above analysis and parametric study are used to optimize the phase-shifter design. With considering a limitation of fabrication accuracy, the optimized microstrip is designed with the substrate of $\varepsilon_{r1} = 10.8$, $H_1 = 10$ mil, and $W = 5$ mil, which gives a characteristic impedance of 64 Ω at 40 GHz. The substrate used has a metal thickness of 17 μm with rms surface roughness of 0.3–1.4 μm. It is shown in Fig. 7(a) that the S-parameter magnitudes of the phase shifter are not much affected at the maximum dielectric perturbation at 90 V. This indicates that the phase is changed while the characteristic impedance is kept fairly constant during the perturbation. Thru-reflect-line (TRL) calibration is used to remove the effect of the coaxial-to-microstrip line transitions. Up to 40 GHz, the maximum perturbation-added loss is about 1.5 dB, and the total loss is about 4 dB for a phase shifting of 480°, as shown in Fig. 8. The return loss S_{11} is less than -10 dB over most of the frequency range. In Fig. 7(b), the calculated loss based on Section II shows very good agreement with the measured data if the mismatch loss ($= 10\log(1-|S_{11}|^2)$) is considered. The small discrepancy near 40 GHz between expected and measured results may be partly caused by an imperfect calibration, surface-mode generation from the microstrip line, and/or the radiation loss at the perturber boundary due to the abrupt transition.

Fig. 8 shows measured differential phase shifts with varying frequencies and PET voltages. There is no deflection (or no perturbation) at 0 V and full downward deflection (or maximum perturbation) at 30 V. This is called a top-down alignment, the reverse of the bottom-up alignment used in [7] and [10]. The calculated phase shift agrees very well with measured data at each PET control voltage. Between 30–90 V of the control voltage, the additional phase shifts becomes small. Thus, the dc bias is required only up to 30 V. This dc voltage can be further decreased if the alignment is improved or a narrower microstrip line and thinner substrate are used.

From Figs. 7 and 8, the optimized PET phase shifter has three advantages compared with the previously reported authors' re-

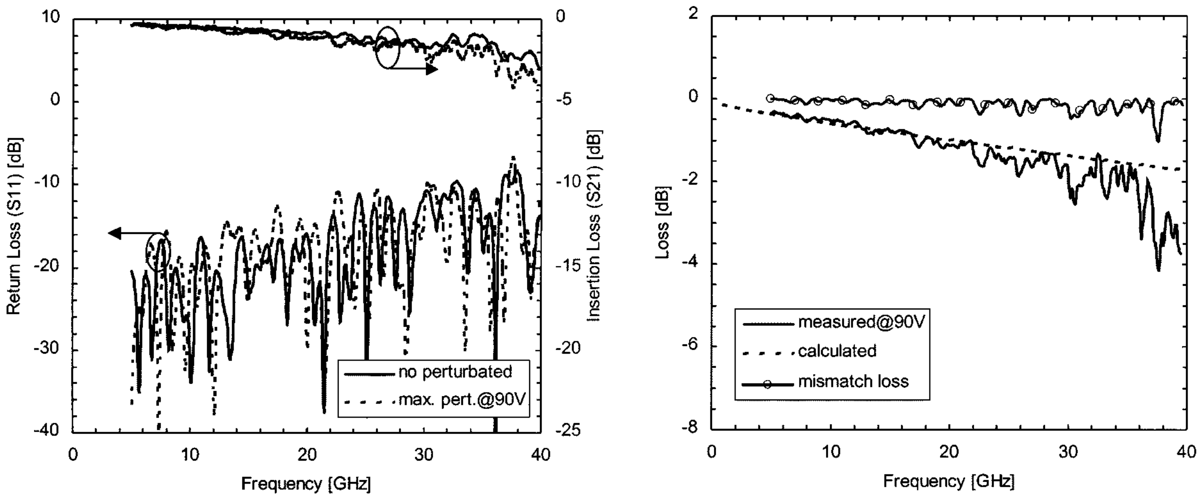

(a) (b)

Fig. 7. Optimized PET phase shifter with $\varepsilon_{r3} = 10.8$, $H_3 = 50$ mil, $L_p = 1.2$ in, $\varepsilon_{r1} = 10.8$, $H_1 = 10$ mil, and $W = 5$ mil. (a) S-parameters with and without dielectric perturbation. (b) Loss comparison between measured and calculated data. The calculated results modified by the mismatch loss agree well with the measured data.

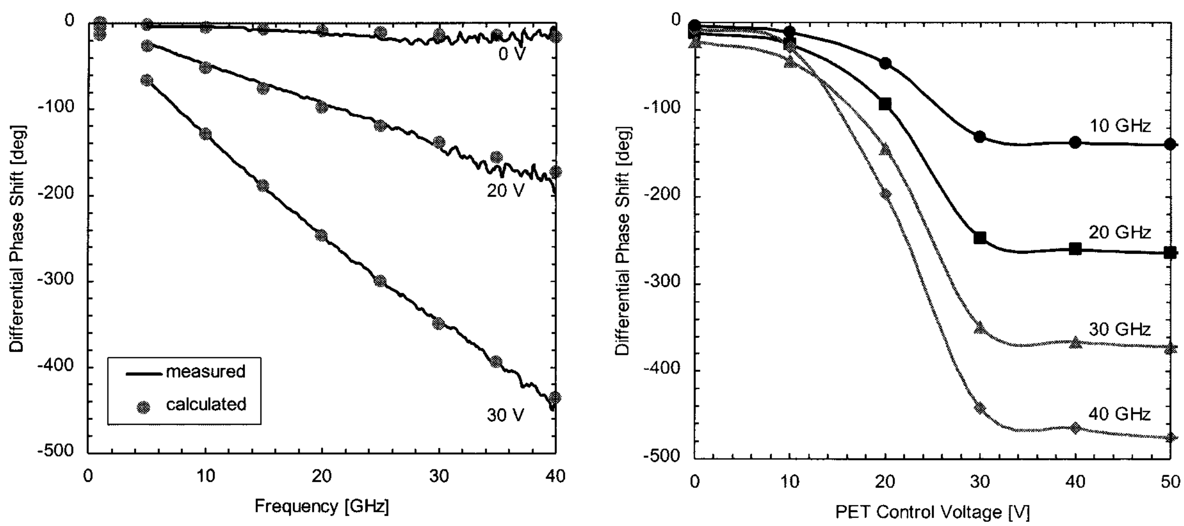

(a) (b)

Fig. 8. Measured differential phase shifts versus: (a) frequency at different PET voltages and (b) PET control voltages at different frequencies with $\varepsilon_{r3} = 10.8$, $H_3 = 50$ mil, $L_p = 1.2$ in, $\varepsilon_{r1} = 10.8$, $H_1 = 10$ mil, and $W = 5$ mil.

sults [7], [10]: the bias voltage range is reduced from 90 to 30 V, the size is reduced from 1.8 to 1.2 in, and the phase-shift curves are more linear versus frequency, even though the S-parameters and phase-shifting performance are similar. In addition, a phase shift/insertion loss ratio of 229°/dB at 25 GHz and 287°/dB at 35 GHz are achieved. The results are better than those reported in [12] and [13].

V. Conclusion

A phase shifter controlled by a PET has been analyzed and optimized. To analyze the multilayer microstrip structure of the PET phase shifter, new ESL equations have been developed and confirmed with the measurements and the SDA of the moment method. The equations have been used for the phase shift and loss calculations. A parametric analysis has been accomplished with ESL and SDA, and optimization guidelines have been suggested. A PET phase shifter has been optimized using this technique to operate at up to 40 GHz with a maximum loss of 4 dB and a phase shift of 480°. Measured results agreed very well with calculations. The optimized phase shifter has the advantages of smaller control voltage, smaller size, and better linearity, as compared with the previously published data.

Acknowledgment

The authors would like to thank M. Li, Texas A&M University, College Station, C. Wang, Texas A&M University, College Station, C. Rodenbeck, Texas A&M University, College Station, and H. Tehrani, Texas A&M University, College Station, for technical assistance and helpful discussion.

References

[1] B. York, A. Nagra, and J. Speck, "Thin-film ferroelectrics: Deposition methods and applications," presented at the IEEE MTT-S Int. Microwave. Symp. Workshop, Boston, MA, June 2000.

[2] S. Lucyszyn and I. D. Robertson, "Synthesis techniques for high performance octave bandwidth 180° analog phase shifters," *IEEE Trans. Microwave Theory Tech.*, vol. 40, pp. 731–740, Apr. 1992.
[3] J. B. L. Rao, D. P. Patel, and V. Krichevsky, "Voltage-controlled ferroelectric lens phased arrays," *IEEE Trans. Antennas Propagat.*, vol. 47, pp. 458–468, Mar. 1999.
[4] C. S. Lee and J. M. Tran, "Coplanar waveguide semiconductor phase shifter," *Microwave Opt. Technol. Lett.*, vol. 10, no. 2, pp. 100–102, Oct. 1995.
[5] S.-S. Lee, A. H. Udupa, H. Erlig, H. Zhang, Y. Chang, D. H. Chang, D. Bhttacharya, B. Tsap, W. H. Steier, L. R. Dalton, and H. R. Fetterman, "Demonstration of a photonically controlled RF phase shifter," *IEEE Microwave Guided Wave Lett.*, vol. 9, pp. 357–359, Sept. 1999.
[6] M.-Y Li and K. Chang, "New tunable phase shifters using perturbed dielectric image lines," *IEEE Trans. Microwave Theory Tech.*, vol. 46, pp. 1520–1523, Oct. 1998.
[7] T.-Y. Yun and K. Chang, "A low loss time-delay phase shifter controlled by piezoelectric transducer to perturb microstrip line," *IEEE Microwave Guided Wave Lett.*, vol. 10, pp. 96–98, Mar. 2000.
[8] R. C. Buchanan, Ed., *Ceramic Materials for Electronics*. New York: Marcel Dekker, 1986.
[9] T.-Y. Yun and K. Chang, "An electronically tunable photonic bandgap resonator controlled by piezoelectric transducer," in *IEEE MTT-S Int. Microwave. Symp. Dig.*, Boston, MA, June 2000, pp. 1445–1447.
[10] ——, "A phased-array antenna using a multi-line phase shifter controlled by a piezoelectric transducer," in *IEEE MTT-S Int. Microwave. Symp. Dig.*, Boston, MA, June 2000, pp. 831–833.
[11] N. K. Das and D. M. Pozar, "Personal computer aided analysis of multiplayer transmission lines (PCAAMT), ver. 1.0,", Amherst, MA, June 1990.
[12] A. S. Nagra and R. A. York, "Distributed analog phase shifters with low insertion loss," *IEEE Trans. Microwave Theory Tech.*, vol. 47, no. 9, pp. 1705–1711, 1999.
[13] A. Borgioli, Y. Liu, A. S. Nagra, and R. A. York, "Low-low distributed MEMS phase shifter," *IEEE Microwave Guided Wave Lett.*, vol. 10, pp. 7–9, Jan. 2000.
[14] N. S. Barker and G. M. Rebeiz, "Optimization of distributed MEMS transmission-line phase shifters U-band and W-band designs," *IEEE Trans. Microwave Theory Tech.*, vol. 48, pp. 1957–1966, Nov. 2000.
[15] J. S. Hayden and G. M. Rebeiz, "2-bit MEMS distributed X-band phase shifters," *IEEE Microwave Guided Wave Lett.*, vol. 10, pp. 540–542, Dec. 2000.
[16] N. K. Das and D. M. Pozar, "A generalized spectral-domain Green's function for multilayer dielectric substrates with application to multilayer transmission lines," *IEEE Trans. Microwave Theory Tech.*, vol. MTT-35, pp. 326–335, Mar. 1987.
[17] ——, "Full-wave spectral-domain computation of material, radiation, and guided wave losses in infinite multilayered printed transmission lines," *IEEE Trans. Microwave Theory Tech.*, vol. 39, pp. 54–63, Jan. 1991.
[18] L.-M. Chou, R. G. Rojas, and P. H. Pathak, "A WH/GSMT-based full-wave analysis for planar transmission lines embedded in multilayered dielectric substrates," *IEEE Trans. Microwave Theory Tech.*, vol. 43, pp. 119–130, Mar. 1995.
[19] A. K. Verma and R. Kumar, "New empirical unified dispersion model for shielded-, suspended-, and composite-substrate microstrip line for microwave and mm-wave applications," *IEEE Trans. Microwave Theory Tech.*, vol. 46, pp. 1187–1192, Aug. 1998.
[20] M. Kirschning and R. H. Jansen, "Accurate model for effective dielectric constant of microstrip with validity up to millimeter-wave frequencies," *Electron. Lett.*, vol. 18, no. 6, pp. 272–273, Mar. 1982.
[21] B. Bhat and S. K. Koul, "Lumped capacitance, open-circuit end effects, and edge-capacitance of microstrip-like transmission lines for microwave and millimeter-wave applications," *IEEE Trans. Microwave Theory Tech.*, vol. MTT-32, pp. 433–439, May 1984.
[22] R. Crampagne, M. Ahmadpanah, and J.-L. Guiradu, "A simple method for determining the Green's function for a large class of MIC lines having multilayered dielectric structures," *IEEE Trans. Microwave Theory Tech.*, vol. MTT-26, pp. 82–87, Feb. 1978.
[23] B. Bhat and S. K. Koul, "Unified approach to solve a class of strip and microstrip-like transmission lines," *IEEE Trans. Microwave Theory Tech.*, vol. MTT-30, pp. 679–686, May 1982.
[24] A. K. Verma, A. Bhupal, Z. Rostamy, and G. P. Srivastava, "Analysis of rectangular patch antenna," *IEICE Trans. Commun. (Japan)*, vol. E74, no. 5, pp. 1270–1276, May 1991.
[25] W. J. Getsinger, "Microstrip dispersion model," *IEEE Trans. Microwave Theory Tech.*, vol. MTT-21, pp. 34–39, Jan. 1973.
[26] I. J. Bahl and S. S. Stuchly, "Analysis of a microstrip covered with a lossy dielectric," *IEEE Trans. Microwave Theory Tech.*, vol. MTT-28, pp. 104–109, Feb. 1980.
[27] R. A. Pucel, D. J. Masse′, and C. P. Hartwig, "Losses in microstrip," *IEEE Trans. Microwave Theory Tech.*, vol. MTT-16, pp. 342–350, June 1968.
[28] E. O. Hammerstad and Ø. Jensen, "Accurate models for microstrip computer-aided design," in *IEEE MTT-S Int. Microwave. Symp. Dig.*, 1980, pp. 407–409.
[29] A. K. Verma and G. H. Sadr, "Unified dispersion model for multilayer microstrip line," *IEEE Trans. Microwave Theory Tech.*, vol. 40, pp. 1587–1591, July 1992.
[30] G.-S. Choi, H.-S. Kim, and G.-H. Choi, "A study on position control of piezoelectric actuators," in *IEEE Int. Ind. Electron. Symp. Dig.*, vol. 3, Guimarães, Portugal, 1997, pp. 851–855.
[31] J. M. Cruz-Hernández and V. Hayward, "Reduction of major and minor hysteresis loops in a piezoelectric actuator," in *Proc. 37th IEEE Decision Contr. Dig.*, Tampa, FL, Dec. 1998, pp. 4320–4325.

Tae-Yeoul Yun (S'99) received the B.S.E.E. degree from the Kyung-Pook National University, Kyung-Pook,Korea, in 1987 the M.S.E.E. degree from the Korea Advanced Institute of Science and Technology (KAIST), Seoul, Korea, in 1989, and the Ph.D. degree in electrical engineering from Texas A&M University, College Station, TX, in 2001.

From 1989 to 1996, he was with the Optical Telecommunication System Group, Electronics and Telecommunications Research Institute (ETRI), Taejon, Korea, where he developed 2.5- and 10-Gb/s systems. He has authored or co-authored over 40 technical papers. His research interests are passive and active microwave circuits, phased-array antenna systems, and high-speed optical telecommunication devices and systems.

Kai Chang (S'75–M'76–SM'85–F'91) received the B.S.E.E. degree from the National Taiwan University, Taipei, Taiwan, R.O.C., in 1970, the M.S. degree from the State University of New York at Stony Brook, in 1972, and Ph.D. degree from The University of Michigan at Ann Arbor, in 1976.

From 1972 to 1976, he was with the Microwave Solid-State Circuits Group, Cooley Electronics Laboratory, The University of Michigan at Ann Arbor, where he was a Research Assistant. From 1976 to 1978, he was with Shared Applications Inc., Ann Arbor, MI, where he was involved with computer simulation of microwave circuits and microwave tubes. From 1978 to 1981, he was with the Electron Dynamics Division, Hughes Aircraft Company, Torrance, CA, where he was involved in the research and development of millimeter-wave solid-state devices and circuits, power combiners, oscillators, and transmitters. From 1981 to 1985, he was with TRW Electronics and Defense, Redondo Beach, CA, where he was a Section Head involved with the development of state-of-the-art millimeter-wave integrated circuits and subsystems, including mixers, voltage-controlled oscillators (VCOs), transmitters, amplifiers, modulators, upconverters, switches, multipliers, receivers, and transceivers. In August 1985, he joined the Electrical Engineering Department, Texas A&M University, College Station, as an Associate Professor, and became a Professor in 1988. In January 1990, he became an E-Systems Endowed Professor of Electrical Engineering. He has authored and co-authored several books, including *Microwave Solid-State Circuits and Applications* (New York: Wiley, 1994), *Microwave Ring Circuits and Antennas* (New York: Wiley, 1996), *Integrated Active Antennas and Spatial Power Combining* (New York: Wiley, 1996), and *RF and Microwave Wireless Systems* (New York: Wiley, 2000). He has served as the Editor of the four-volume *Handbook of Microwave and Optical Components* (New York: Wiley, 1989 and 1990). He is the Editor of *Microwave and Optical Technology Letters* and the Wiley Book Series on "Microwave and Optical Engineering." He has also authored or co-authored over 350 technical papers and several book chapters in the areas of microwave and millimeter-wave devices, circuits, and antennas. His current interests are in microwave and millimeter-wave devices and circuits, microwave integrated circuits, integrated antennas, wide-band and active antennas, phased arrays, microwave power transmission, and microwave optical interactions.

Dr. Chang was the recipient of the 1984 Special Achievement Award presented by TRW, the 1988 Halliburton Professor Award, the 1989 Distinguished Teaching Award, the 1992 Distinguished Research Award, and the 1996 Texas Engineering Experiment Station (TEES) Fellow Award presented by Texas A&M University.